INTERNATIONAL JOURNAL FOR NUMERICAL METHODS IN FLUIDS, VOL. 21, 205–222 (1995)

ACCURATE COMPUTATION OF CONVECTIVE TRANSPORT IN TRANSIENT TWO-PHASE FLOW

M. J. ANDREWS

Department of Mechanical Engineering, Texas A&M University, College Station, TX 77843-3123, U.S.A.

SUMMARY

The Van Leer method for the computation of convective fluxes is extended to two-phase flow. By preventing spurious undershoots and overshoots, the scheme preserves physical realism while maintaining high-order accuracy. This is particularly important for two-phase flows, since phase exchange terms are typically a function of volume fraction products and numerical diffusion can incorrectly mix the two phases. The scheme described here is constructed to guarantee that the sum of the volume fractions is always unity and that the volume fractions are always greater than or equal to zero. Various test problems are computed to demonstrate the accuracy of the method and to show how the scheme might be incorporated in existing computational methods. In addition to multiphase flow applications, setting equal phase velocities results in a volume marker scheme that is well suited to single-phase interface tracking problems.

KEY WORDS: two-phase; Van Leer; convective transport; volume fractions; momentum; interface tracking

INTRODUCTION

There are few known exact solutions of the governing equations of two-phase flow and those that are known represent simple physical systems that have limited practical application. Consequently, investigators of two-phase flow fall back on experimentally determined correlations and more recently solutions of the governing equations obtained by computer. This paper addresses the problem of minimizing numerical diffusion associated with numerical representation of the convective terms in the two-phase governing equations. It is well known that numerical schemes that discretize the convective terms with an upwind procedure suffer from excessive numerical diffusion; the use of a higher-order scheme can substantially reduce this problem but can also lead to oscillations causing non-physical undershoots or overshoots. The implication of these results for two-phase flow calculations is particularly significant for the computation of the convection of phase volume fraction (mass). If an upwind procedure is used for volume fraction advection, then numerical diffusion tends to smear gradients of volume fraction. Typical two-phase exchange terms involve the product of volume fractions, so smearing produces finite values in those exchange terms, leading to numerically induced source terms and consequent inaccuracies throughout the calculation. If a naive higher-order scheme is used for volume fraction advection, then non-physical oscillations might appear in the volume fraction profiles, as well as overshoots or undershoots, so that volume fractions may be less than zero or greater than unity, which again would produce unphysical phase exchange source terms.

This paper describes the use of the Van Leer method[1] for the computation of convective fluxes as applied to the convective transport of phase volume fraction (mass) and phase momentum in two-phase flow. The Van Leer scheme prevents spurious oscillations while maintaining a high order of numerical

CCC 0271–2091/95/030205–18

Received 11 February 1994
Revised 19 December 1994

accuracy. Application of the Van Leer scheme to volume fraction advection is not straightforward, since the individual phase volume fractions are linked by the relation $f_1 + f_2 = 1$, and for the incompressible calculations considered here, care must be taken to compute velocity and pressure fields that simultaneously satisfy joint continuity and momentum equations. The scheme is described in two dimensions and may be easily extended to three dimensions.

MATHEMATICAL EQUATIONS FOR SOLUTION

For the present purposes the following set of two-phase flow equations is employed to demonstrate the new solution procedures:

$$\text{continuity} \quad \frac{\partial(f_i\rho_i)}{\partial t} + \frac{\partial(f_i\rho_i u_i)}{\partial x} + \frac{\partial(f_i\rho_i v_i)}{\partial y} = 0, \tag{1}$$

$$u\text{-momentum} \quad \frac{\partial(f_i\rho_i u_i)}{\partial t} + \frac{\partial(f_i\rho_i u_i^2)}{\partial x} + \frac{\partial(f_i\rho_i u_i v_i)}{\partial y} = -f_i\frac{\partial p}{\partial x} + F_i(u_1 - u_2) + f_i B_{i,x}, \tag{2}$$

$$v\text{-momentum} \quad \frac{\partial(f_i\rho_i v_i)}{\partial t} + \frac{\partial(f_i\rho_i v_i u_i)}{\partial x} + \frac{\partial(f_i\rho_i v_i^2)}{\partial y} = -f_i\frac{\partial p}{\partial y} + F_i(v_1 - v_2) + f_i B_{i,y}, \tag{3}$$

where $i = 1$ or 2, the first or second phase. The phase variables are volume fractions, f_1, x- and y-direction velocities u_i and v_i respectively, and a pressure shared by both fluids, p. There are seven independent variables and six equations; the seventh equation to close the set is $f_1 + f_2 = 1$. The momentum equations (1) and (2) also contain x- and y-direction body force terms such as gravity and F_i is a drag coefficient which satisfies $F_1 = -F_2$.

NUMERICAL SOLUTION PROCEDURE

The governing equations presented above are a coupled set of partial differential equations for which there exist several solution procedures.[2,3] The present work solves transient problems and uses an explicit approach that serves to demonstrate the new transport procedures while being simple to code and validate. The governing equations are solved by a fractional time step technique which at each time step performs an advection calculation followed by a Lagrangian source term update. The Lagrangian update is presented next and this is followed by a detailed description of the advection step for volume fraction and momentum.

Lagrangian momentum source term updates

Discretization of the Lagrangian momentum equations gives the following relations for phase velocities:

$$\begin{aligned} u^*_{i,\mathrm{e}} &= u^{n+1/2}_{i,\mathrm{e}} + \frac{\Delta t}{\rho_i \Delta x}(p^n_{\mathrm{P}} - p^n_{\mathrm{E}}) + \frac{F^{n+1}_{i,\mathrm{e}}(u^{n+1/2}_{1,\mathrm{e}} - u^{n+1/2}_{2,\mathrm{e}})}{\rho_i f^n_{i,\mathrm{e}}} + g_x, \\ v^*_{i,\mathrm{n}} &= v^{n+1/2}_{i,\mathrm{n}} + \frac{\Delta t}{\rho_i \Delta y}(p^n_{\mathrm{P}} - p^n_{\mathrm{N}}) + \frac{F^{n+1}_{i,\mathrm{n}}(v^{n+1/2}_{1,\mathrm{n}} - v^{n+1/2}_{2,\mathrm{n}})}{\rho_i f^n_{i,\mathrm{n}}} + g_y. \end{aligned} \tag{4}$$

In the present formulation a linear drag law is used with

$$F^{n+1}_{1,\mathrm{n}} = -F^{n+1}_{2,\mathrm{n}} = C_{\mathrm{D}}\rho_1 f^{n+1}_{1,\mathrm{n}} f^{n+1}_{2,\mathrm{n}}, \qquad F^{n+1}_{1,\mathrm{e}} = -F^{n+1}_{2,\mathrm{e}} = C_{\mathrm{D}}\rho_1 f^{n+1}_{1,\mathrm{e}} f^{n+1}_{2,\mathrm{e}}.$$

Extension to quadratic forms is straightforward and described later. The $n+\frac{1}{2}$ superscript refers to a value from the advection calculation, while the asterisk denotes an intermediate value that does not necessarily satisfy continuity. The subscripts refer to spatial position, as shown in Figure 1, and a staggered arrangement of momentum and mass cells is used. Body force terms are constant and taken as components of gravity in later test problems. The momentum cell values for volume fractions $f_{i,e}^{n+1}$ and $f_{i,n}^{n+1}$ may be taken in several ways but should be the same as used in the pressure correction equation; here an upwind formulation is used based on the face cell velocity. A desirable constraint in two-phase flow is that the net volume flux should be conserved, i.e.

$$\delta V_e - \delta V_w + \delta V_n - \delta V_s = 0, \tag{5}$$

with $\delta V_e = \Delta t \Delta y (u_{1,e}^{n+1} f_{1,e}^{n+1} + u_{2,e}^{n+1} f_{2,e}^{n+1})$ and $\delta V_n = \Delta t \Delta x (v_{1,n}^{n+1} f_{1,n}^{n+1} + v_{2,n}^{n+1} f_{2,n}^{n+1})$, where $n+1$ refers to a new time level value. This is the two-phase analogue of the single-phase situation, but if the velocities from (4) are used in (5), there is no guarantee that the net volume flux will be zero. Following the single-phase SIMPLE[4] practice, phase velocity corrections are defined so that $u_{i,e}^{n+1} = u_{i,e}^{*} + \Delta u_{i,e}$ and $v_{i,n}^{n+1} = v_{i,n}^{*} + \Delta v_{i,n}$ and the new pressure $p_P^{n+1} = p_P^n + \Delta p_P$, where Δp is a pressure correction. By substituting these expressions for $n+1$ into equations (4) and then subtracting (4) evaluated with the asterisk, we arrive at the velocity influence equations

$$\Delta u_{i,e} = \frac{\Delta t}{\rho_i \Delta x}(\Delta p_P - \Delta p_E), \qquad \Delta v_{i,n} = \frac{\Delta t}{\rho_i \Delta y}(\Delta p_P - \Delta p_N), \tag{6}$$

with similar expressions for the west and south faces. Now substituting these expressions into (5) gives a Poisson equation for pressure corrections,

$$a_P \Delta p_P + a_E \Delta p_E + a_W \Delta p_W + a_N \Delta p_N + a_S \Delta p_S = -D, \tag{7}$$

with, for example,

$$a_E = -\frac{\Delta t \Delta y}{\Delta x}\left(\frac{f_{1,e}^{n+1}}{\rho_1} + \frac{f_{2,e}^{n+1}}{\rho_2}\right),$$

and D evaluated as (5) using the asterisked velocity values, with face volume fractions taken as upwind values. The Poisson equation (7) is then solved and the pressure corrections are inserted into (6) to provide updated $n+1$ velocities and pressures that simultaneously satisfy the momentum equations (4) and net volume flux (5). The Poisson solver used in this work is a Gauss–Seidel method iterated until the sum of the absolute mass residuals (the right side of (7)) over all the cells is less than some

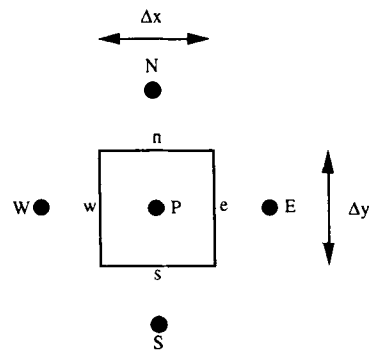

Figure 1. Cartesian control volume showing neighbouring East, West, North and South cells and east, west, north and south faces

prescribed value. This two-phase calculation procedure closely resembles the single-phase one, but here no iteration is required because the source update momentum equation is linear; if we had implicit convection or diffusion terms or a quadratic velocity-dependent drag coefficient, then iteration would be needed.

Transport procedures

The two-dimensional transport procedures are split into an x-step followed by a y-step; this is followed by a y–x calculation at the next time step. This fractional splitting simplifies the calculation to two one-dimensional updates and lends itself to high-order calculation of cell fluxes with the Van Leer method. However, in a two-phase application, special care must be taken to conserve net volume, the completeness of the volume fractions and their positivity. The next subsection describes the advection of phase volume fraction (or phase mass for this incompressible case) within these constraints and is followed by a compatible procedure for phase momentum.

Advection of phase volume fraction. The following describes the advection of phase volume over a time step; for an incompressible two-phase flow this procedure may also be interpreted as advection of phase mass, while for a single-phase interface tracker it is the advection of the marker fluid. The continuity equations (1) are represented by the finite volume balance equations

$$x\text{-step} \quad f^*_{i,\mathrm{P}} V^*_{\mathrm{P}} = f^n_{i,\mathrm{P}} V^n_{\mathrm{P}} + \delta V_{i,\mathrm{w}} - \delta V_{i,\mathrm{e}}, \tag{8}$$

$$y\text{-step} \quad f^{n+1}_{i,\mathrm{P}} V^{n+1}_{\mathrm{P}} = f^*_{i,\mathrm{P}} V^*_{\mathrm{P}} + \delta V^*_{i,\mathrm{s}} - \delta V^*_{i,\mathrm{n}}. \tag{9}$$

These balance equations relate the intermediate (asterisked) and new $(n+1)$ phase volumes to the phase volumes fluxed over the cell faces. Attention is focused on the x-step; the y-step proceeds in a similar fashion using the latest asterisked values.

Phase volume fluxes are calculated as $\delta V_{i,\mathrm{e}} = \Delta y \Delta t \tilde{u}_{i,\mathrm{e}} \tilde{f}_{i,\mathrm{e}}$, where the tilde denotes cell face values computed as below. An intermediate cell volume V^*_{P} is computed by adding the x-step phase volume equations (8) to give

$$V^*_{\mathrm{P}} = V^{\mathrm{cell}}_{\mathrm{P}} + \delta V_{\mathrm{w}} - \delta V_{\mathrm{e}}, \tag{10}$$

where δV_{w} and δV_{e} are the net volumes fluxed over the east and west faces respectively. Since $f^n_{1,\mathrm{P}} + f^2_{2,\mathrm{P}} = 1$, this ensures that $f^*_{1,\mathrm{P}} + f^*_{2,\mathrm{P}} = 1$. Similarly, addition of the phase volume equations for the y-step (9) yields

$$V^{n+1}_{\mathrm{P}} = V^*_{\mathrm{P}} + \delta V_{\mathrm{s}} - \delta V_{\mathrm{n}}, \qquad f^{n+1}_{1,\mathrm{P}} + f^{n+1}_{2,\mathrm{P}} = 1. \tag{11}$$

If the net volume fluxes are chosen to be those used in the pressure iteration (7), then since the joint continuity equation was iterated to convergence, we have $\delta V_{\mathrm{w}} - \delta V_{\mathrm{e}} + \delta V_{\mathrm{s}} - \delta V_{\mathrm{n}} = 0$; using this relationship in (10) and (11) gives $V^{n+1}_{\mathrm{P}} = V^n_{\mathrm{P}}$, so the net cell volume is conserved, but also along the way we have satisfied $f^*_{1,\mathrm{P}} + f^*_{2,\mathrm{P}} = 1$ and $f^{n+1}_{1,\mathrm{P}} + f^{n+1}_{2,\mathrm{P}} = 1$. It remains to calculate the individual phase volume fluxes for equations (8) and (9).

The x-step phase volume fluxes are chosen to satisfy

$$\Delta y \Delta t (\tilde{u}_{1,\mathrm{e}} \tilde{f}_{1,\mathrm{e}} + \tilde{u}_{2,\mathrm{e}} \tilde{f}_{2,\mathrm{e}}) = \delta V_{\mathrm{e}} \tag{12}$$

and similarly for west face fluxes. The net volume flux δV_{e} is saved from the pressure iteration and so

is available. To satisfy (12), the cell face velocities are calculated as $\tilde{u}_{1,e} = u^n_{1,e} + \Delta u$ and $\tilde{u}_{2,e} = u^n_{2,e} + \Delta u$, with the velocity adjustment Δu determined to satisfy (12) as

$$\Delta u = \frac{\delta V_e - \Delta y \Delta t (u^n_{1,e} \tilde{f}_{1,e} + u^n_{2,e} \tilde{f}_{2,e})}{\Delta y \Delta t (\tilde{f}_{1,e} + \tilde{f}_{2,e})}. \tag{13}$$

The face values $\tilde{f}_{1,e}$ and $\tilde{f}_{2,e}$ are determined as the average value on the face for a profile advected across the face at speeds $\tilde{u}_{1,e}$ and $\tilde{u}_{2,e}$ respectively; see Figure 2. The result for $\tilde{f}_{1,e}$ is

$$\tilde{f}_{1,e} = \tilde{f}_{1,\text{upwind}} + \text{sign}(\varepsilon_{1,e}) \frac{1 - \varepsilon_{1,e}}{2} \Delta x D_{1,e}, \tag{14}$$

where $\varepsilon_{1,e} = \delta V_{1,e} / V^n_{1,\text{upwind}} = \tilde{f}_{1,e} V^{\text{cell}}_{\text{upwind}}$ and upwind values are taken according to the sign of $\varepsilon_{1,e}$. The derivative is evaluated following Van Leer as

$$D_{1,e} = S \min\left\{ |D|, \quad \frac{2|\Delta_w|}{\Delta x}, \quad \frac{2|\Delta_e|}{\Delta x} \right\}, \tag{15}$$

where

$$\Delta_w = f^n_{1,P} - f^n_{1,W}, \qquad \Delta_e = f^n_{1,E} - f^n_{1,P}, \qquad S = \begin{cases} 1 & \text{if } \Delta_e \text{ and } \Delta_w > 0, \\ -1 & \text{if } \Delta_e \text{ and } \Delta_w < 0, \\ 0 & \text{otherwise.} \end{cases}$$

Van Leer limiters have been used in (15) to limit the gradient of the volume fraction profile, thereby preventing spurious oscillations. The representation of the gradient of the cell profile D determines the accuracy of the representation.

If $D = 0$, the cell profile takes a constant upwind value and so this scheme is subsequently referred to as 'first-order'.

If $D = (\Delta_e + \Delta_w)/2\Delta x$, the cell profile is assumed linear. The gradient is computed with a central difference and so this scheme is subsequently referred to as 'second-order'.

Following Youngs,[5] if

$$D = \begin{cases} (1 + |\varepsilon_{1,e}|)\Delta_w/3 + (2 - |\varepsilon_{1,e}|)\Delta_e/3 & \text{for } \varepsilon_{1,e} \geqslant 0, \\ (1 + |\varepsilon_{1,e}|)\Delta_e/3 + (2 - |\varepsilon_{1,e}|)\Delta_w/3 & \text{for } \varepsilon_{1,e} < 0, \end{cases}$$

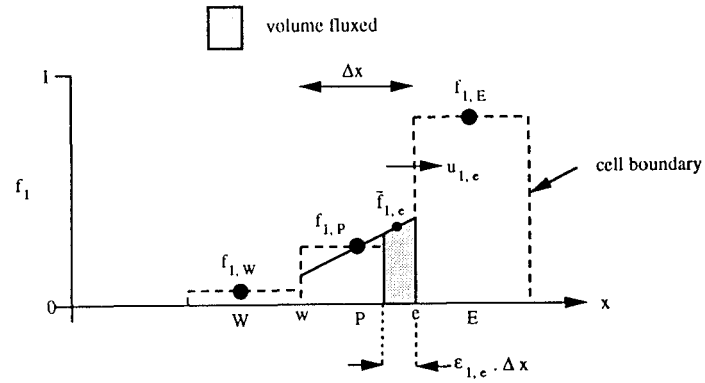

Figure 2. Phase volume fluxed over east face

this scheme is referred to as 'third-order'. If $|\varepsilon_{1,e}| = \frac{1}{2}$, this third-order scheme reduces to the central difference scheme, so we might expect the two schemes to be of similar accuracy.

To complete this phase volume fraction scheme, the appearance of Δu via $\varepsilon_{1,e}$ in equation (14) for $\tilde{f}_{1,e}$ means that the evaluation of Δu in equation (13) must be iterated with equation (14); in the present work iteration continued until $|\Delta u^{k+1} - \Delta u^k| \leq 10^{-8}$.

In summary, the x-step phase volume fraction computation for a cell is performed as follows:

1. Compute the net east volume flux using the same procedure as in the pressure iteration.
2. Initialize $\Delta u = 0$.
3. Compute $\tilde{f}_{1,e}$ using (14) and (15) and similarly for $\tilde{f}_{2,e}$.
4. Compute a new Δu using (13) and return to step 3 until converged.
5. Use $\tilde{u}_{i,e}$ and $\tilde{f}_{i,e}$ to compute phase volume fluxes $\delta V_{i,e}$.
6. Insert $\delta V_{i,e}$ and previous computed west volume fluxes into (8) for the new volume fractions $f^*_{i,P}$.

The y-step proceeds in a similar fashion using v-velocities and resulting in updated phase volume fractions $f^{n+1}_{i,P}$.

Advection of phase momentum. First- and second-phase advections are independent, unlike the volume fractions, and so it suffices to detail only the first phase; the second being identical but with subscript 1 replaced by subscript 2. Since the phase densities are constant in this work, they have been dropped from the following momentum equations. As before, the update is split into an x-step followed by a y-step as follows:

$$x\text{-step} \quad V^*_{1,e}u^*_{1,e} = V^n_{1,e}u^n_{1,e} + \delta V_{1,P}\tilde{u}_{1,P} - \delta V_{1,E}\tilde{u}_{1,E}, \tag{16}$$

$$y\text{-step} \quad V^{n+1/2}_{1,e}u^{n+1/2}_{1,e} = V^*_{1,e}u^*_{1,e} + \delta V_{1,se}\tilde{u}^*_{1,se} - \delta V_{1,ne}\tilde{u}^*_{1,ne}, \tag{17}$$

where the subscripts refer to the staggered u-velocity cell and the tilde refers to values taken on the cell faces; in particular, $\tilde{u}_{1,E}$ is the mean value of u_1 on the east face of the cell during the time step. The superscript $n + \frac{1}{2}$ indicates that this is only a partial update to be followed by the Lagrangian force calculation. The phase volumes and fluxes are calculated as $V^n_{1,e} = (V^n_{1,P} + V^n_{1,E})/2$ and $\delta V_{1,E} = (\delta V_{1,e} + \delta V_{1,ee})/2$ respectively, where the scalar phase volumes and fluxes are available from the volume fraction update described above. The intermediate phase volume is calculated as

$$V^*_{1,e} = V^n_{1,e} + \delta V_{1,P} - \delta V_{1,E},$$

which, as in the volume fraction calculation, ensures $V^{n+1/2}_{i,e} = V^n_{i,e}$. The calculation of $\tilde{u}_{1,E}$ uses a similar high-order approximation to that used for volume fractions:

$$\tilde{u}_{1,E} = u^n_{1,\text{upwind}} + \text{sign}(\varepsilon_{1,E})\frac{1 - |\varepsilon_{1,E}|}{2}\Delta x D_{1,E}, \tag{18}$$

where $\varepsilon_{1,E} = \delta V_{1,E}/V^n_{1,\text{upwind}}$, with upwind values determined by the sign of $\varepsilon_{1,E}$. The dertivative is found from

$$D_{1,E} = S \min\left\{|D|, \quad \frac{2|\Delta_P|}{\Delta x}, \quad \frac{2|\Delta_E|}{\Delta x}\right\}, \tag{19}$$

with

$$\Delta_P = u^n_{1,e} - u^n_{1,w}, \qquad \Delta_E = u^n_{1,ee} - u^n_{1,e}, \qquad S = \begin{cases} 1 & \text{if } \Delta_P \text{ and } \Delta_E > 0, \\ -1 & \text{if } \Delta_P \text{ and } \Delta_E < 0, \\ 0 & \text{otherwise.} \end{cases}$$

Again Van Leer limiters have been applied to prevent spurious oscillations.

As for the phase volume, the cell velocity profile gradient D may take various forms yielding similarly formulated 'first-order', 'second-order' and 'third-order' schemes.

In summary, the x-step phase momentum computation for a cell is performed as follows.

1. Compute momentum cell volumes and volume fluxes using values available from the volume fraction calculation.
2. Compute cell face velocities using equation (18).
3. Compute intermediate cell phase momentum using equation (16).

The y-step proceeds in a similar fashion using v-velocities and resulting in updated cell phase momentum.

Limitations and extensions of the advection schemes. The explicit procedures above are restricted as follows.

(i) The Courant condition $\varepsilon < 1$ prevails, limiting the time step by the cell size and velocity.
(ii) The formulation employs a uniform grid. This restriction may be removed by taking an appropriate representation of the cell profile gradient in equations (15) and (19).
(iii) Fixed flux boundary conditions (either zero or non-zero) may be applied by assigning boundary volume fluxes or momentum fluxes in equations (8) and (9) or equations (16) and (17). Similarly, cyclic boundary conditions associate values required after the last cell with the first and before the first cell with the last.
(iv) Single-phase advection may be readily computed with these procedures by setting $u_1 = u_2$ and $v_1 = v_2$. The velocity correction Δu of equation (13) is then zero and so no iteration is required; the volume fraction may now be used as a fluid marker as will be demonstrated below. In the momentum advection algorithm, phase mass and phase mass flux are exchanged for fluid mass and fluid mass flux in a single-phase calculation.

TEST PROBLEMS

To demonstrate the new transport procedures, several test problems are described and then solved. The chosen problems have been divided into single-phase problems where the fluid marker technique can be applied, and two-phase problems where there is slip between the phases and the two-phase flow procedures are appropriate. Each problem is solved using combinations of first-, second- and third-order schemes as listed in Table I.

Each problem description includes a brief introduction to the problem, terms in the governing equations, initial and boundary conditions and expected results. This is followed by details of the computation such a grid, time step, initial values, convergence and iteration parameters. The results are then presented and discussed. All the problems have been solved on a 486DX33 PC computer. Typical run times for each problem are given in Table II.

Table I. Test cases for all test problems

Case	Volume fractions	Momentum
1	1st order	1st order
2	2nd order	1st order
3	2nd order	2nd order
4	3rd order	3rd order

Single-phase test problems: Rayleigh–Taylor instability

Problem description

The problem is to predict the growth of a single Rayleigh–Taylor instability[6] at the interface of different density fluids. Initially a heavy fluid (ρ_2) overlays a lighter one (ρ_1) and gravity drives the growth of a single-wavelength perturbation. The problem is depicted in Figure 3. To give the problem an element of physical realism, the densities and dimensions are those from the Rayleigh–Taylor mixing experiments of Andrews and Spalding,[7] where brine and water were used as the two fluids. For the purposes of this problem the two-dimensional Euler equations (1) and (2) for a single phase describe the growth of the instability with body forces $B_x = 0{\cdot}0$ and $B_y = \rho g$, so the y-axis is aligned with the vertical.

The initial conditions are

$$\rho = \rho_2 = 1{\cdot}1 \times 10^3 \text{ kg m}^{-3} \text{ (brine)} \quad \text{for } y > Y_L/2 + A_0 \cos(k_0 x),$$

$$\rho = \rho_1 = 1{\cdot}0 \times 10^3 \text{ kg m}^{-3} \text{ (water)} \quad \text{for } y \leq Y_L/2 + A_0 \cos(k_0 x),$$

where $0 \leq y \leq Y_L$ (= 0·36 m) and $0 \leq x \leq X_L$ (= 0·25 m). The initial amplitude and wave number of the perturbation are $A_0 = \lambda/100$ and $k_0 = 2\pi/\lambda$ respectively, with $\lambda = X_L$. The initial values for velocities are zero and pressure takes a hydrostatic distribution.

The boundary conditions are as follows: at $x = 0$ and $x = X_L$, $u = 0$; at $y = 0$ and $y = Y_L$, $v = 0$.

In the absence of viscosity, linear stability analysis[8] gives the amplitude A of the perturbation growing as $A = A_0 \cosh(n_\lambda t)$, with the exponential growth rate given by

$$n_\lambda^2 = \frac{2\pi g}{\lambda} \frac{\rho_1 - \rho_2}{\rho_1 + \rho_2}$$

The e-folding time $1/n_\lambda$ for this problem is 0·292 s.

Table II. Typical run times (seconds) for each problem

Problem	Test case 2
2D Rayleigh–Taylor	253
2D Kelvin–Helmholtz	107
1D sedimentation	46
2D unstable mixing	105

Computational details

The volume fraction calculation was employed as a marker for the fluid densities, so that the local density was calculated as $\rho = f_1\rho_1 + f_2\rho_2$. For convenience the fluid densities were set as $\rho_1 = 1{\cdot}0$ and $\rho_2 = 1{\cdot}1$. A reduced pressure form of the gravitational term has been used,[9] with $B_y = (\rho_2 - \rho_1)g$.

For the tests reported here, the computational grid comprised 26 uniformly spaced cells in the y-direction and 18 uniformly spaced cells in the x-direction. The problem has been run to a simulation time of 2 s with 100 time steps of 0·02 s and with a mass residual tolerance of 10^{-4}. Preliminary work showed that this time step gave results independent of time step and mass residual. A check of the cell Courant number showed a maximum of 0·6, in keeping with the expected maximum value of 1·0.

The initial density distribution was set via the volume fractions as

$$f_1 = \begin{cases} \varepsilon & \text{if } y > Y_L/2 + A_0 \cos(k_0 x), \\ 1 - \varepsilon & \text{if } y \leqslant Y_L/2 + A_0 \cos(k_0 x), \end{cases}$$

where $\varepsilon = 10^{-3}$. For cells that contain the perturbation, the perturbation is integrated to provide a volume fraction for the fluid in the cell.

Results

Figure 3 shows the calculated time history development of the instability as indicated by the fluid marker using the second-order volume fraction and momentum schemes. The figure shows symmetry about the vertical centreline, implying that the velocity fields must also be symmetrical. The amplitude of the perturbation was measured at $t = 0{\cdot}5$ s using the 0·5 volume fraction contour and assigned a value of 5·08 cm. This corresponds to an e-folding time of 0·29 s, in good agreement with the expected value of 0·292 s.

Figure 4 shows the relative merits of the four different schemes of Table I. Comparison of the various schemes shows that using a second- or third-order scheme substantially improves the accuracy of the calculation, resulting in significantly more roll-up of the perturbation and the smallest spacing between contours. It is useful to note the significant increase in roll-up upon increasing the order of the momentum calculation; this point is reinforced in the next problem. However, there is little improvement to be gained by going from second to third order.

Single phase test problems: Kelvin–Helmholts instability

Problem description

Kelvin–Helmholtz instability is another fundamental fluid flow instability,[8] and may occur when two fluid layers flow past one another. If the interface between the fluid streams is perturbed, the perturbation grows as a Kelvin–Helmholtz instability, rolling up the interface. The problem then is to

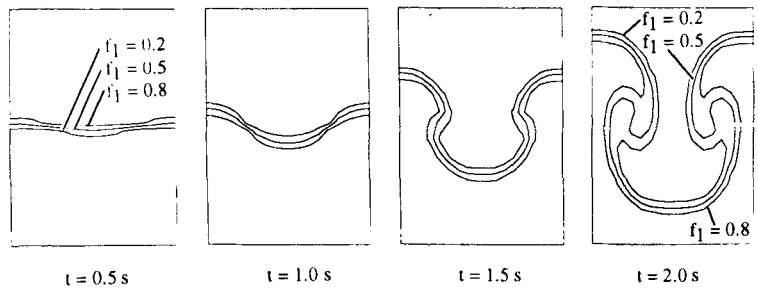

Figure 3. Development of a Rayleigh–Taylor instability calculated using second-order volume fraction and momentum schemes

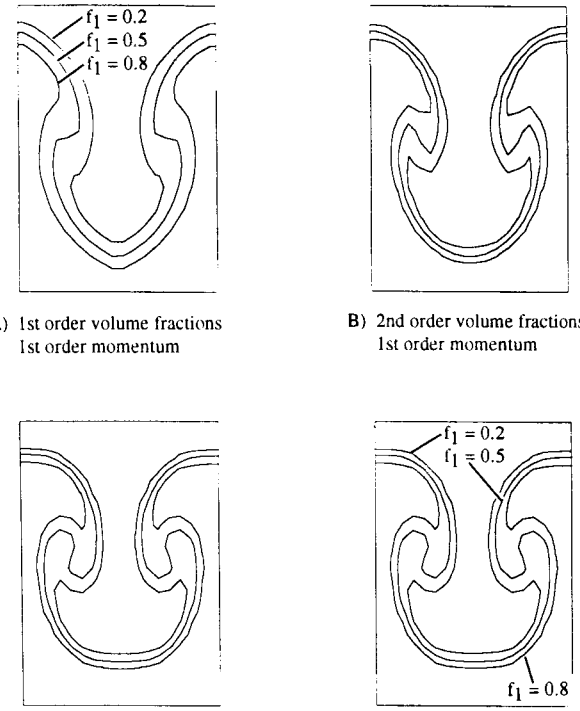

A) 1st order volume fractions
1st order momentum

B) 2nd order volume fractions
1st order momentum

C) 2nd order volume fractions
2nd order momentum

D) 3rd order volume fractions
3rd order momentum

Figure 4. Computed Rayleigh–Taylor instability at $t = 2$ s calculated with different schemes

predict the growth of a single Kelvin– Helmholtz instability in a fluid of uniform density and the problem specification is close to that of Rosenhead.[10]

The two-dimensional Euler equations are used to simulate the instability; however, there are no body forces and the fluid has a uniform density $\rho_1 = \rho_2 = 1$.

The initial conditions are as follows. The fluid velocities are $u = \bar{u} + u'$ and $v = v'$, where $\bar{u}$ is the stream velocity given by

$$\bar{u} = \begin{cases} -u_\infty & \text{for } 0 \leqslant y \leqslant Y_L/2 \quad \text{and } 0 \leqslant x \leqslant X_L, \\ u_\infty & \text{for } Y_L/2 < y \leqslant Y_L \quad \text{and } 0 \leqslant x \leqslant X_L, \end{cases}$$

with $u_\infty = 1{\cdot}0$ m s^{-1} and $X_L = Y_L = 1$ m. The velocity perturbations to the steady state are $u' = -\partial\varphi/\partial y$ and $v' = \partial\varphi/\partial x$, where the streamfunction is given by

$$\varphi = \hat{u} \cos(kx) \frac{e^{-k|\delta_y|}}{1 - e^k} \begin{cases} 1 - e^{2k(1/2+|\delta_y|)} & \text{if } \delta_y \leqslant 0, \\ 1 - e^{2k(1/2-|\delta_y|)} & \text{if } \delta_y > 0, \end{cases}$$

with $\hat{u} = 0{\cdot}2u_\infty$, $k = 2\pi/X_L$ and $\delta_y = y - Y_L/2$. In the calculations that follow, the volume fractions mark the fluid that initially moves to the right, $\bar{u} > 0$, as $f_1 = 0{\cdot}0$ and that to the left as $f_1 = 1{\cdot}0$.

The boundary conditions are as follows. At $y = 0$ and $y = Y_L$, $v = 0$. Cyclic boundaries prevail in the x-direction, so that $u(x = 0) = u(x = X_L)$. The streamfunction has been constructed to satisfy these boundary conditions.

Computational details

A total of 256 square cells were used to cover the computational domain, 16 in each direction. The time step used was 0·01 s to ensure that the Courant number $\varepsilon = u_\infty t/\Delta y$ was less than 0·5.

The stream velocity was set as defined above but with a linear velocity gradient across the cells straddling the line separating the fluid streams. This was found to promote the development of the instability. The velocity perturbations on the east and north faces of a computational cell are set respectively as

$$u'_e = -\left(\frac{\varphi_{ne} - \varphi_{se}}{\Delta y}\right), \qquad v'_n = -\left(\frac{\varphi_{ne} - \varphi_{nw}}{\Delta x}\right),$$

where 'ne' denotes the northeast corner of a cell. This practice ensured that the velocity perturbations satisfied continuity. A zero initial pressure field was set and an initial volume fraction of

$$f_1 = \begin{cases} 1 - 10^{-3} & \text{if } 0 \leqslant y \leqslant Y_L/2, \\ 10^{-3} & \text{if } Y_L/2 < y \leqslant Y_L, \end{cases} \quad \text{for } 0 \leqslant x \leqslant X_L.$$

Boundary conditions were specified as in the problem statement.

Convergence of the pressure iteration calculation was determined by setting a total mass residual of 10^{-4}; a residual check similar to the one for the Rayleigh–Taylor problem was performed and found this tolerance satisfactory.

Results

Figure 5 shows the calculated growth of a Kelvin–Helmholtz instability using second-order volume fractions and momentum. An expected symmetry between the top and bottom tongues as they are swept downstream may be observed. Figure 6 provides a comparison of the different schemes. The figures reaffirm that the second- or third-order schemes give the most accurate results (most structure and closest contours). Comparison of the results using first-order momentum with those using second-order momentum reveals that numerical diffusion in the calculation of momentum transport has the effect of damping out the growth of the instability, thus demonstrating the need for an accurate calculation of momentum transport. The computed roll-up shape resembles that computed by Rosenhead;[10] a discrepancy in the time of roll-up may be attributed to the initial flat marker interface in the present calculations (Rosenhead perturbed vortices on the interface by 0·1 m).

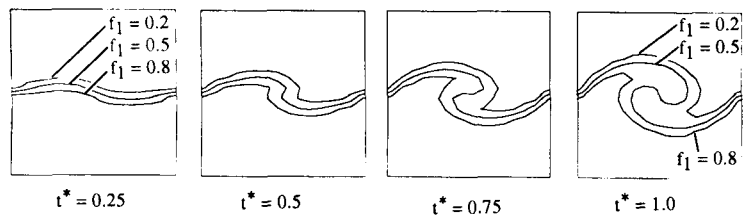

Figure 5. Development of a Kelvin–Helmholtz instability calculated using second-order volume fraction and momentum schemes for non-dimensional time $t^* = u_\infty t/\lambda$

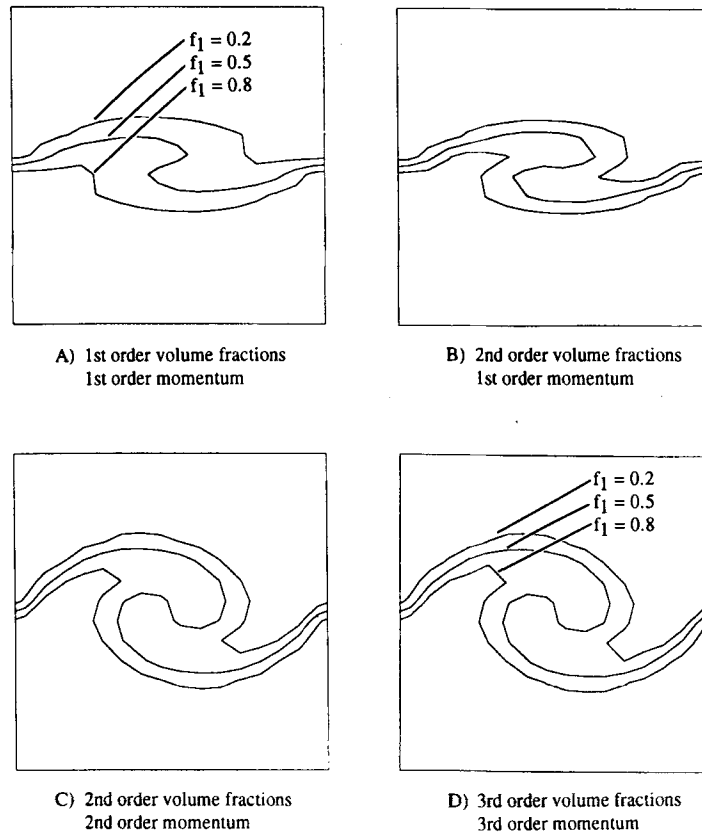

Figure 6. Computed Kelvin–Helmholtz instability at $u_\infty t/\lambda = 1$ calculated with different schemes

Two-phase test problems: One-dimensional sedimentation

Problem description

The physical situation comprises two fluids of differing densities initially lying at rest with the heavy fluid ($\rho = \rho_2$) overlying the light fluid ($\rho = \rho_1$); see Figure 7. Driven by gravity, the heavy fluid sediments through the light fluid, forming a mixed region that expands to fill the remaining volume. This physical situation is that explored in experiments by Andrews and Spalding.[7] Their fluids and dimensions are adopted here: $\rho_2 = 1{\cdot}1 \times 10^3$ kg m^{-3} (brine), $\rho_1 = 1{\cdot}0 \times 10^3$ kg m^{-3} (water), with the height of the domain as 0·36 m. Because the densities are close, a comparison with an analytical solution is possible; also, since the results are sensitive to numerical diffusion in the volume fraction equations, this problem is a good test of the volume fraction transport equations.

In this one-dimensional two-phase problem we solve the y-direction continuity and momentum equations (1) and (3) with the u-velocities zero (identical results were obtained upon solving the problem in the x-direction). The body force terms are $B_{1,y} = \rho_1 g$ and $B_{2,y} = \rho_2 g$. The interphase friction term is taken as $F = C_f f_1 f_2 \rho_1$, with $C_f = 20{\cdot}0$.

The initial conditions are

$$v_1 = v_2 = 0 \quad \text{for } 0 \leqslant y \leqslant Y_L/2, \qquad f_1 = \begin{cases} 1 & \text{for } 0 \leqslant y \leqslant Y_L/2, \\ 0 & \text{for } Y_L/2 < y \leqslant Y_L, \end{cases}$$

with $Y_L = 0{\cdot}36$ m. Pressure takes a hydrostatic distribution.

The boundary conditions are as follows: at $y = 0$ and $y = Y_L$, $v_1 = v_2 = 0$.

Andrews[11] gives an approximate analytical solution for this problem. The following calculations compute from the initial position to a time of 2·4 s, sufficient for the volume fraction profile to spread across the domain. The solution for this period is

$$f_1 = \begin{cases} \frac{1}{2}(1 - \delta_y/v_\infty t) & \text{for } -v_\infty t \leqslant y \leqslant v_\infty t, \\ 1 & \text{for } \delta_y < -v_\infty t, \\ 0 & \text{for } \delta_y > v_\infty t, \end{cases}$$

where $\delta_y = y - Y_L/2$ and v_∞ is a terminal velocity given by

$$v_\infty = -g(\rho_2 - \rho_1)/C_f\rho_1,$$

which takes a value of $4{\cdot}905 \times 10^{-2}$ m s^{-1} and gives a mixing width $2v_\infty t$ of 0·2354 m.

Computational details

As in the Rayleigh–Taylor problem, a reduced pressure formulation was used to promote convergence of the pressure iteration; the body force terms used were $B_{1,y} = 0{\cdot}0$ and $B_{2,y} = (\rho_2 - \rho_1)g$. A total of 40 uniformly spaced cells span the computational domain and a time step of 0·02 s was used to ensure the Courant condition $v_\infty \Delta t/\Delta y < 0{\cdot}5$.

Zero initial velocities and a hydrostatic pressure were set. The initial volume fractions were

$$f_1 = \begin{cases} 1 - 10^{-3} & \text{for } 0 \leqslant y \leqslant Y_L/2, \\ 10^{-3} & \text{for } Y_L/2 < y \leqslant Y_L, \end{cases}$$

with zero mass and momentum fluxes across the upper and lower boundaries.

Convergence of the pressure iteration calculation was determined by setting a total mass residual of 10^{-4}; a residual check was performed and found this tolerance satisfactory.

Results

Figure 7 shows the volume fraction profiles at $t = 0$, 1·2 and 2·4 s calculated using second-order volume fraction and momentum formulations. As expected from the analytical solution, a linear volume fraction profile expands through the domain. The figure shows the analytical solution as a solid line and a comparison of computed with analytical results reveals excellent agreement. Figure 8 compares different schemes at $t = 2{\cdot}4$ s and shows that using the first-order upwind scheme for volume fractions introduces significant numerical diffusion into the solution that is strongly reminiscent of experimental mix profiles,[12] but here it is a numerical artefact. To see better the difference between calculated and exact solutions, Figure 9 plots the width of the mixing region, as measured by the distance between $f_1 = 0{\cdot}05$ and $f_1 = 0{\cdot}95$, against time for the first-order, second-order and exact solutions. The figure reveals that the second-order scheme accurately follows the development of the mix width, whereas the first-order scheme overpredicts by approximately 20% at the end of the calculation.

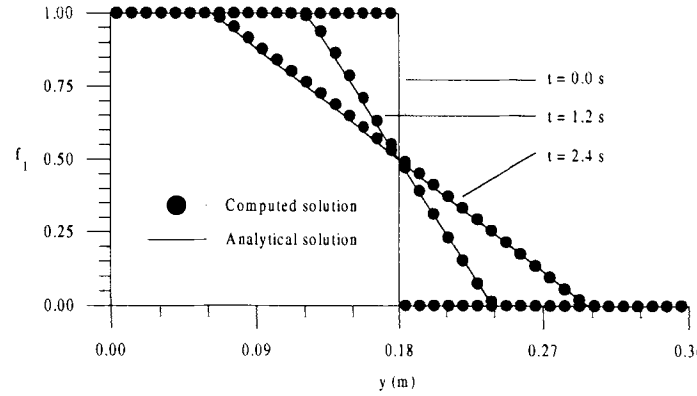

Figure 7. Computed one-dimensional sedimentation calculated using second-order volume fraction and momentum schemes

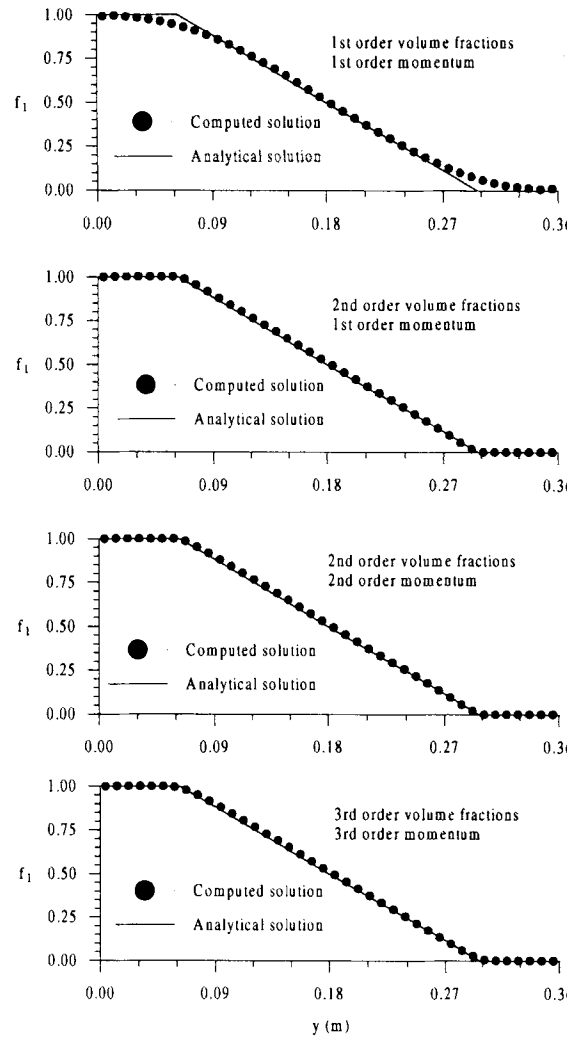

Figure 8. One-dimensional sedimentation first-phase volume fraction profiles at $t = 2{\cdot}4$ s calculated with different schemes

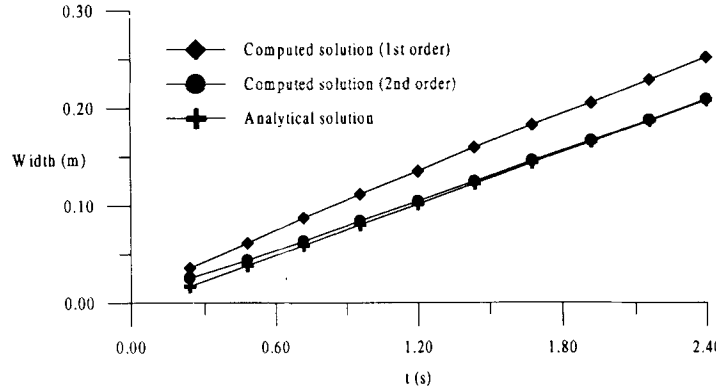

Figure 9. Growth of sediment mixing width computed with different schemes

Two-phase test problems: Overturning in a tilted rectangular cavity

Problem description

The physical situation envisaged for this two-phase test problem resembles that of the Rayleigh–Taylor problem. Initially a heavy fluid ($\rho = \rho_2$) overlies a lighter fluid ($\rho = \rho_1$) in an enclosed rectangular cavity; see Figure 10. It is then supposed that the cavity is instantaneously tilted without imparting any motion to the fluids. As a result the gravitational field is angled in the frame of reference of a level initial interface, causing an overturning motion to develop. Superimposed on the large-scale overturning motion is an interpenetration of the two phases due to mixing being driven by the vertical component of gravity, similar to the one-dimensional test problem above.

The physical motivation for this problem comes from the 'tilted' Rayleigh–Taylor mixing experiments of Andrews and Spalding[7] in which the two fluids are brine and water and the overturning motion is initiated by quickly inverting a tilted two-dimensional tank.

The governing equations to be solved for this problem are equations (1)–(3) with the components of the body force given by $B_{i,x} = -\rho_i g \sin\beta$ and $B_{i,y} = \rho_i g \sin\beta$ for $i = 1$ and 2, water and brine respectively. The tilt angle β is taken as 3° to conform with the experimental work and the densities are $\rho_1 = 1 \times 10^3$ kg m^{-3} (water) and $\rho_2 = 1{\cdot}1 \times 10^3$ kg m^{-3} (brine). The interphase friction term is again $F = C_f f_1 f_2 \rho_1$, with $C_f = 20{\cdot}0$.

The initial conditions are $u_1 = u_2 = v_1 = v_2 = 0{\cdot}0$ for $0 \leq x \leq X_L$ and $0 \leq y \leq Y_L$, with the domain dimensions taken from the experiment, $X_L = 0{\cdot}25$ m and $Y_L = 0{\cdot}36$ m. Pressure takes a hydrostatic distribution and the volume fraction field is given by

$$f_1 = \begin{cases} 1 & \text{if } 0 \leqslant y \leqslant Y_L/2 \quad \text{and } 0 \leqslant x \leqslant X_L, \\ 0 & \text{if } Y_L/2 < y \leqslant Y_L \quad \text{and } 0 \leqslant x \leqslant X_L. \end{cases}$$

The boundary conditions are as follows: at $x = 0$ and $x = X_L$, $u_1 = u_2 = 0{\cdot}0$; at $y = 0$ and $y = Y_L$, $v_1 = v_2 = 0{\cdot}0$.

The overturning motion is generated by a Rayleigh–Taylor perturbation of wavelength $2X_L$ and the e-folding time is then 0·4 s. This result will be used to compare with the growth of the perturbation taken as the contour $f_1 = 0{\cdot}5$.

Computational details

A reduced pressure form of the gravity terms has been used with $B_{1,x} = B_{1,y} = 0$, $B_{2,x} = -(\rho_2 - \rho_1)g \sin\beta$ and $B_{2,y} = (\rho_2 - \rho_1)g \cos\beta$. A total of 160 uniformly spaced cells were

used, with 10 in the x-direction and 16 in the y-direction. The time step was 0·02 s, since the maximum velocities in this problem are similar to those of the Rayleigh–Taylor problem.

The initial velocities were zero with a hydrostatic pressure and the initial volume fractions were

$$f_1 = \begin{cases} 1 - 10^{-3} & \text{if } 0 \leqslant y \leqslant Y_L/2 \text{ and } 0 \leqslant x \leqslant X_L, \\ 10^{-3} & \text{if } Y_L/2 < y \leqslant Y_L \text{ and } 0 \leqslant x \leqslant X_L. \end{cases}$$

Boundary conditions were set by specifying zero mass and momentum fluxes over the domain boundaries.

The problem is expected to have similar velocities and volume fluxes to the Rayleigh–Taylor problem and so convergence of the pressure iteration calculation was determined by setting a total volume residual of 10^{-4}.

Results

Figure 10 shows the development of the overturning and also the expansion of a mix region between the two fluids computed using the second-order scheme. This computed result agrees qualitatively with the observations of Andrews and Spalding.[7] The e-folding time was determined from the amplitude of the perturbation at $t = 0{\cdot}1$ and 0·2 s as 0·39 s, in good agreement with the expected value of 0·4 s. Figure 11 shows that the second- and higher-order schemes again have similar accuracy and are substantially more accurate than the first-order scheme.

CONCLUSIONS

New procedures have been described for solving phase volume and momentum transport in one- and two-dimensional two-phase flow. The procedures use an explicit formulation that permits the use of Van Leer limiters with higher-order representation of fluxes, thus preventing non-physical oscillations.

Four test problems have been presented and solved with the new solution procedures. The test problems have been used to demonstrate that the solution procedures work correctly. It has been shown that an upwind, first-order scheme results in significant numerical diffusion. The numerical diffusion is substantially reduced upon using a second-order scheme, but little further improvement is achieved with a third-order scheme. The two-dimensional single-phase problems have shown the need for high-order momentum advection to prevent strong numerical damping of the computed solution.

The use of a high-order volume fraction and momentum advection calculation is recommended when solving the equations of transient two-phase flow and the present Van Leer limited schemes work well.

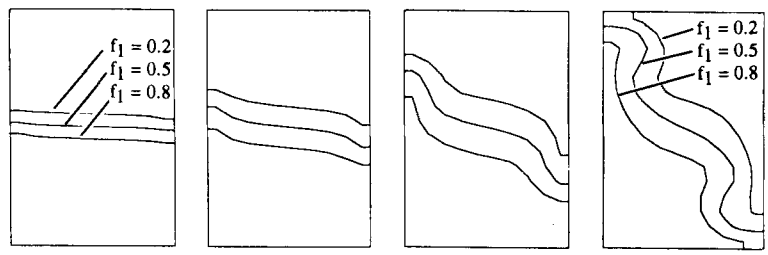

Figure 10. Computed tilted cavity problem using second-order volume fraction and momentum schemes

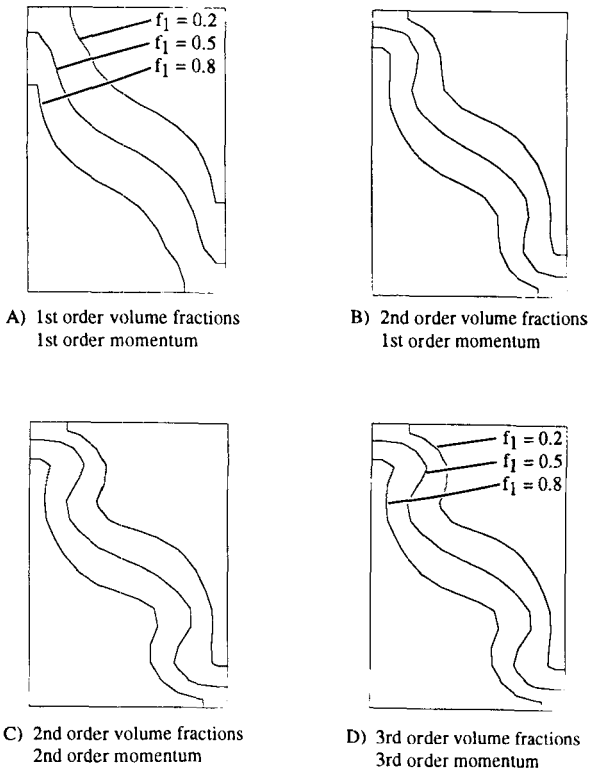

Figure 11. Tilted cavity first-phase volume fraction contours computed at $t = 2$ s with different schemes

ACKNOWLEDGEMENTS

This work has been supported in part by an Engineering Excellence Grant from Texas A&M University. Thanks are also due to Dr D. L. Youngs of AWE Aldermaston for many insightful comments during the work.

APPENDIX: NOMENCLATURE

$B_{i,x}$	body force for phase i in the x-direction
C_F	interphase friction coefficient
ε_{max}	maximum Courant number for calculation based on $\varepsilon_{max} = v_{fluid}\Delta t/\Delta x$
f_i	volume fraction of phase i
F	interphase friction
g	gravitational acceleration, $-9{\cdot}81$ m s^{-2}
p	pressure
P	denotes centre of scalar cell
t, Δt	time and time step (s)
u	x-direction velocity (m s^{-1})
v	y-direction velocity (m s^{-1})
V	volume (m^3)
x, Δx	x-co-ordinate and size of computational cell in x-direction (m)
X_L	length of calculation domain in x-direction (m)
y, Δy	y-co-ordinate and size of computational cell in y-direction (m)
Y_L	length of calculation domain in y-direction (m)

REFERENCES

1. B. Van Leer, 'Towards the ultimate conservative difference scheme, IV. A new approach to numerical convection', *J. Comput. Phys.*, **23**, 276–299 (1977).
2. F. H. Harlow and A. A. Amsden, 'Numerical calculation of multiphase fluid flow', *J. Comput. Phys.*, **17**, 19–52 (1975).
3. D. B. Spalding, 'The calculation of free-convection phenomena in gas–liquid mixtures', in N. Afgan and D. B. Spalding (eds), *Turbulent Buoyant Convection*, Hemisphere, Washington, DC, 1977, pp. 569–586.
4. S. V. Patankar, *Numerical Heat Transfer and Fluid Flow*, Hemisphere, Washington, DC, 1980.
5. D. L. Youngs, 'Accurate numerical methods for volume-fraction transport in one-dimensional multifluid flow', *AWRE Report 44/92/29*, 1984.
6. G. I. Taylor, 'The instability of liquid surfaces when accelerated in a direction perpendicular to their planes, I', *Proc. R. Soc. Lond. A***201**, 192–196 (1950).
7. M. J. Andrews and D. B. Spalding, 'A simple experiment to investigate two-dimensional mixing by Rayleigh–Taylor instability', *Phys. Fluids A***2** 922–927 (1990).
8. S. Chandrasekhar, *Hydrodynamic and Hydromagnetic Stability*, Oxford University Press, Oxford, 1961.
9. A. H. A. Baghdadi, 'Numerical modelling of two-phase flow with interphase slip', *Ph.D. Thesis*, University of London, 1979.
10. L. Rosenhead, 'The formation of vortices from a surface of discontinuity', *Proc. R. Soc. Lond. A***134**, 170–192 (1931).
11. M. J. Andrews, 'Turbulent mixing by Rayleigh–Taylor instability', *Ph.D. Thesis*, University of London, 1986.
12. D. M. Snider and M. J. Andrews, 'Rayleigh–Taylor and shear driven mixing with an unstable thermal stratification', *Phys. Fluids A***6**, 3324–3334 (1994).